Structure of human cortisol-producing cytochrome P450 11B1 bound to the breast cancer drug fadrozole provides insights for drug design

Received for publication, October 10, 2018, and in revised form, November 12, 2018 Published, Papers in Press, November 13, 2018, DOI 10.1074/jbc.RA118.006214

Simone Brixius-Anderko[‡] **and Emily E. Scott**[‡§1]

From the Departments of [‡]*Medicinal Chemistry and* [§]*Pharmacology and the Program in Biophysics, University of Michigan, Ann Arbor, Michigan 48109*

Edited by F. Peter Guengerich

Human cytochrome P450 11B1 (CYP11B1) is responsible for the final step generating the steroid hormone cortisol, which controls stress and immune responses and glucose homeostasis. CYP11B1 is a promising drug target to manage Cushing's disease, a disorder arising from excessive cortisol production. However, the design of selective inhibitors has been hampered because structural information for CYP11B1 is unavailable and the enzyme has high amino acid sequence identity (93%) to a closely related enzyme, the aldosterone-producing CYP11B2. Here we report the X-ray crystal structure of human CYP11B1 (at 2.1 Å resolution) in complex with fadrozole, a racemic compound normally used to treat breast cancer by inhibiting estrogen-producing CYP19A1. Comparison of fadrozole-bound CYP11B1 with fadrozole-bound CYP11B2 revealed that despite conservation of the active-site residues, the overall structures and active sites had structural rearrangements consistent with distinct protein functions and inhibition. Whereas fadrozole binds to both CYP11B enzymes by coordinating the heme iron, CYP11B2 binds to the *R* enantiomer of fadrozole, and CYP11B1 binds to the *S* enantiomer, each with distinct orientations and interactions. These results provide insights into the cross-reactivity of drugs across multiple steroidogenic cytochrome P450 enzymes, provide a structural basis for understanding human steroidogenesis, and pave the way for the design of more selective inhibitors of each human CYP11B enzyme.

Human steroidogenesis involves six different cytochrome P450 (CYP)[2] enzymes, including CYP11B1 (11β-hydroxylase), CYP11B2 (aldosterone synthase), and CYP19A1 (aromatase). CYP11B1 and CYP11B2 perform the final steps in biosynthesis of the glucocorticoid cortisol and mineralocorticoid aldosterone, respectively, whereas CYP19A1 produces estrogenic sex steroids (Fig. S1). Alterations in any of these steroidogenic P450 enzymes can cause human disease. The major human glucocorticoid cortisol regulates several catabolic and signaling pathways, including glucose homeostasis and stress and immune responses (1–3). Excess CYP11B1 cortisol production results in Cushing's disease with suppressed immune response, obesity, muscular weakness, hypertension, depression, and infertility (4–6). Aldosterone produced by CYP11B2 regulates water and electrolyte homeostasis (7). Overproduction, called primary hyperaldosteronism, causes high blood pressure, one of the most common cardiovascular diseases (8, 9). Estrogens control female development and fertility but can promote breast cancer proliferation, and selective inhibitors of CYP19A1 treat estrogen-responsive breast cancer (10). Selective inhibitors of CYP11B1 or CYP11B2 are of similar clinical interest (11–17) for Cushing's disease and hypertension. The development of such inhibitors has been impeded by the 93% amino acid sequence identity between them and their similar steroid-binding functionality. Although structures of membrane proteins are difficult to obtain, several are available of CYP11B2 with its physiological substrate 11-deoxycorticosterone and two nonselective inhibitors. However, there are no CYP11B1 structures to identify differences that can be exploited for clinical drug design or understand differences in enzymatic activity. Although CYP11B1 homology models were generated from the CYP11B2 structures (18–20), these highlight similarities more than differences. Thus, the structural basis for distinctions in CYP11B enzyme function is unknown, impeding drug design.

Results and discussion

CYP11B1 characterization

To obtain structural data for human CYP11B1, the enzyme was engineered to omit the N-terminal signaling sequence, recombinantly expressed, and solubilized and purified with detergent. Titrations of CYP11B1 and similarly produced CYP11B2 (21) with their respective substrates 11-deoxycortisol and 11-deoxycorticosterone (Fig. S2) revealed a blue shift in absorbance associated with substrate binding in the active site displacing the water normally on the heme iron (type I interaction). When reconstituted with NADPH and adrenodoxin reductase and adrenodoxin to deliver electrons, both CYP11B1

Initial generation of the CYP11B constructs was supported by National Institutes of Health Grant R37 GM076343. Expression, purification, characterization, and structure determination was supported by startup funds from the University of Michigan. The authors declare that they have no conflicts of interest with the contents of this article. The content is solely the responsibility of the authors and does not necessarily represent the official views of the National Institutes of Health.

This article contains Figs. S1–S5.

The atomic coordinates and structure factors (code 6M7X) have been deposited in the Protein Data Bank (http://wwpdb.org/).

[1] To whom correspondence should be addressed: Dept. of Medicinal Chemistry, University of Michigan, 428 Church St., Ann Arbor, MI 48109. Tel.: 734-764-3530; E-mail: scottee@umich.edu.

[2] The abbreviations used are: CYP, cytochrome P450; PDB, Protein Data Bank; LB, lysogeny broth; TB, terrific broth; IPTG, isopropyl β-D-1-thiogalactopyranoside; PMSF, phenylmethylsulfonyl fluoride; CV, column volumes; Ni-NTA, nickel-nitrilotriacetic acid.

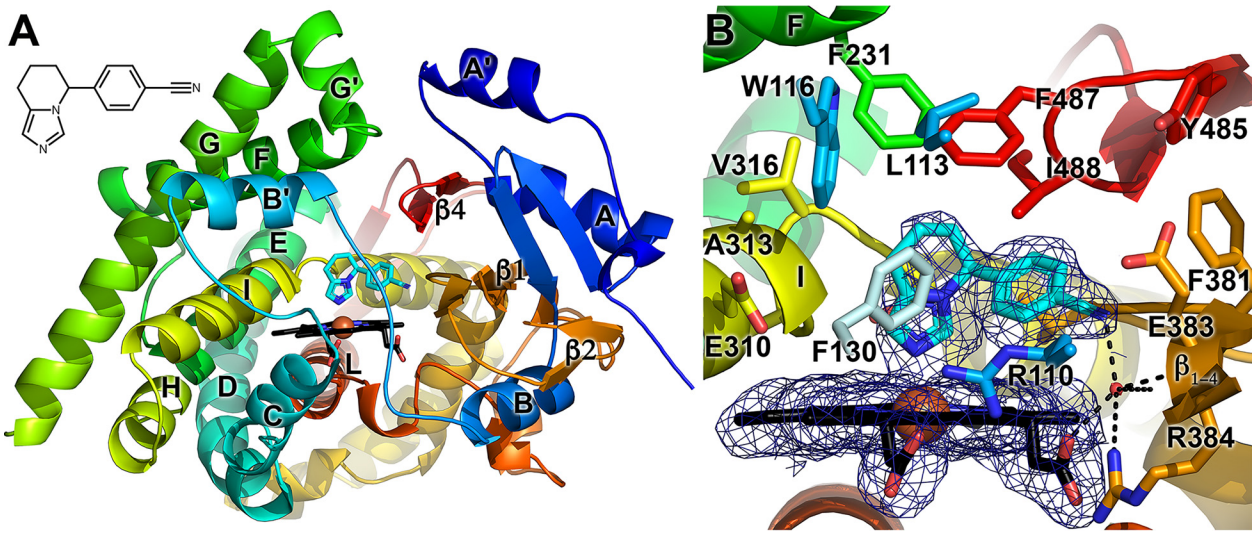

Figure 1. CYP11B1 structure overview (*A*) and active sites (*B*). In both, the enzyme is shown in *rainbow colors* from *blue* at the N terminus to *red* at the C terminus. The heme is shown as *black sticks* with the iron as a *rust sphere*. The inhibitor fadrozole (*structure inset*) is shown in *cyan sticks*. In *B*, water is shown as a *small red sphere* with atoms within hydrogen bonding distance indicated by *black dashed lines*.

(Fig. S3) and CYP11B2 (21) produce their respective cortisol and aldosterone products. Thus, both recombinant enzymes are fully functional. CYP11B1 and CYP11B2 both bound the racemic breast cancer drug fadrozole with a red shift in absorbance, consistent with fadrozole nitrogen coordinating the heme iron, replacing the water (type II interaction; Fig. S2). For comparison, fadrozole is reported to bind its intended CYP19A1 target with similar spectral changes and a K_d of 16 nM, compared with 9 nM for CYP11B1 and 370 nM for CYP11B2, respectively (21). Thus, although fadrozole is used clinically as breast cancer drug inhibiting CYP19A1, it can have off-target effects on both CYP11B enzymes but serves as a starting point for more selective inhibitors.

Structure of CYP11B1 bound to the inhibitor fadrozole

A 2.1 Å X-ray structure of CYP11B1 co-crystallized with the nonselective fadrozole inhibitor (PDB entry 6M7X) reveals the characteristic cytochrome P450 fold (Fig. 1*A*). Consistent with binding studies, fadrozole binds in the CYP11B1 active site with a nitrogen of the imidazole ring coordinated directly to the heme iron, with the fused ring system oriented almost perpendicularly to the plane of the heme and the benzonitrile directed toward β1 (Fig. 1). Ligand nitrogen binding to the iron is known to provide significant affinity for P450 enzymes, but because the heme is conserved across P450 enzymes, this often contributes to significant nonspecificity, as is the case here, and results in undesirable side effects. Residues surrounding the active site can modify the affinity for individual P450 enzymes. In CYP11B1 (Fig. 1*B*), the nitrile of fadrozole hydrogen bonds to water, forming a network. Atoms within hydrogen-bonding distance of this water include the backbone nitrogen and carbonyl of Glu-383 in β_{1-4}, a side-chain nitrogen of Arg-384, and a heme propionate. Thus, this water (and its interactions with fadrozole) is highly stabilized. The roof of the active site opposite the heme is composed of largely hydrophobic residues compatible with hydrophobic regions of fadrozole.

Comparisons between CYP11B1 and CYP11B2 structures with the inhibitor fadrozole

Remarkably, comparison of the CYP11B2–fadrozole structure with the new CYP11B1–fadrozole complex revealed opposite preferences for the two fadrozole enantiomers. Although both CYP11B1 and CYP11B2 were crystallized with the racemic fadrozole used clinically for breast cancer (22), the density clearly supports CYP11B1 binding of the *S* enantiomer and CYP11B2 binding of the *R* enantiomer (21) (Fig. 2*A*). The *R* enantiomer of a similar compound tested preclinically as an inhibitor of CYP11B2 also binds CYP11B2 in a similar orientation (23). Although the imidazopyridine moiety is similarly oriented, binding the heme iron in both structures (Fig. 2*A*), the benzonitrile projects toward β_{1-4} in CYP11B1 and along the central I helix in CYP11B2, where it interacts instead with Arg-120 (Fig. 2*B*). The basis for preferred binding of distinct enantiomers by CYP11B enzymes is based on unique active-site architectures. Despite all active site residues being *identical* in both CYP11B enzymes, large hydrophobic residues Trp-116, Phe-231, Trp-260, Phe-381, Phe-487, and Ile-488 forming the active site roof differ substantially in placement and orientation. Whereas Trp-116, Trp-260, Ala-313 are spread apart to accommodate the benzonitrile of (*R*)-fadrozole in CYP11B2, they are closer to each other in CYP11B1. On the other side of the active site, differential positioning of Phe-381 and Phe-487 permits CYP11B1 to accommodate the benzonitrile of (*S*)-fadrozole. Previous computational studies suggested CYP11B1 preference for (*S*)-fadrozole, but this was based on a predicted orientation with the benzonitrile moiety directed toward the I helix (24), highlighting the necessity of experimental structures, even when structures of close homologs are available.

Many changes in active-site residue position are due to repositioning of their secondary structure elements. At the overall structural level, CYP11B1 and CYP11B2 are very similar on the proximal side of the heme, but major shifts occur in helices on the distal portions of the enzyme, including helices F–G and

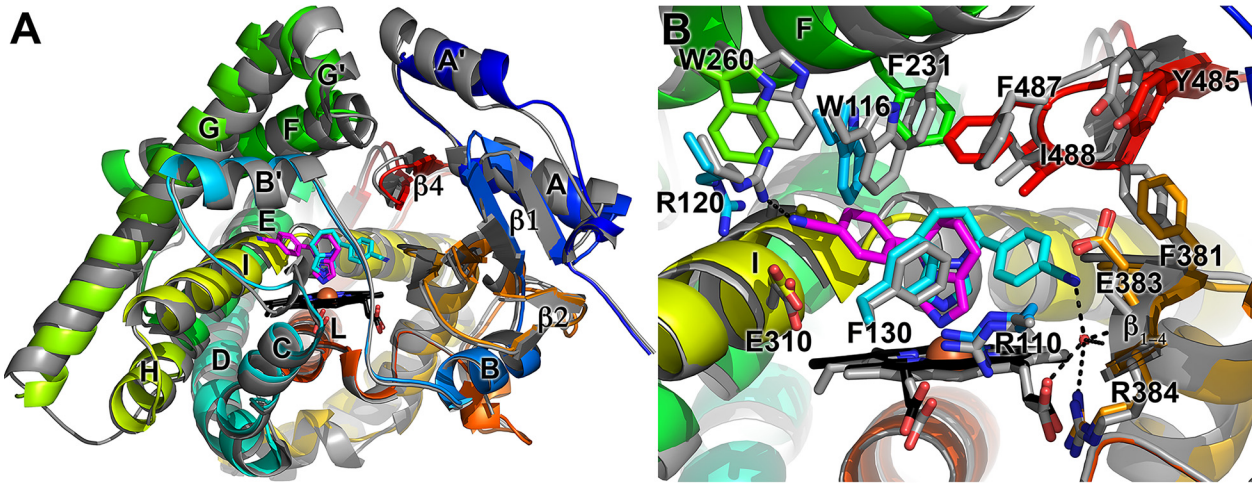

Figure 2. Structural alignments of CYP11B1 and CYP11B2 structures, both with the inhibitor fadrozole. *A*, overview of CYP11B1 (shown as in Fig. 1*A*) and CYP11B2 (*gray ribbons* with *magenta* fadrozole, PDB code 4FDH). *B*, active site showing repositioning of conserved active-site residues to selectively bind (*S*)-fadrozole in CYP11B1 (*cyan*) and (*R*)-fadrozole (*magenta*) in CYP11B2 (PDB code 4FDH).

A′–A (Fig. 2*A*). These elements compose the active site "roof" opposite the heme and are thought to be involved in substrate access to the otherwise buried active site. Thus, residue substitutions outside the active site (Fig. S5) impact overall protein conformation and active site interactions (Fig. 3*A*).

Another notable difference in the CYP11B active sites is the conformation of the central I helix that forms one "wall" of the active site (Fig. 1, *yellow* to *yellow*/*green*). Although this helix often has a slight interruption in the typical hydrogen-bonding pattern as it crosses over the heme, this region is much less helical in CYP11B1, having a break of five amino acid residues compared with two in CYP11B2 (Fig. 3*B*). A shift of this nonhelical region toward the active site center may reduce (*R*)-fadrozole binding. Notably, the identity of residue 320 immediately following this nonhelical region is crucial for the 18-oxidase function of CYP11B2 (25) and may be important in differential binding and orientation of the respective substrates. Notably, introducing CYP11B1 residues into the CYP11B2 helices H (G288S) and I (L301P, E302D, and A320V) increased 11β-hydroxylation efficiency for 11-deoxycortisol (25–27). Whereas residues 288, 301, and 302 are far from the active site and cause little difference at the backbone level, the larger CYP11B1 Val-320 correlates with different rotamers of the flanking Phe-193 and Phe-321 and shifts in the β_4 system and beyond (Fig. 3*B*).

Structural revelation of CYP11B disparate preferences for fadrozole enantiomers is consistent with functional results. (*R*)-Fadrozole, also known as FAD286, has 5-fold selectivity for CYP11B2 over CYP11B1 in rat adrenal cortical preparations (28). As such, (*R*)-fadrozole was a promising compound in preclinical studies for hypertension caused by hyperaldosteronism. In contrast, the *S* enantiomer is reported to be the active CYP19A1-inhibiting agent in breast cancer treatment (29) and is clearly preferred by CYP11B1 (22). A fluorinated version of (*R*)-fadrozole called LCI699 or osilodrostat is the first CYP11B1-inhibiting compound in clinical trials for the treatment of excess cortisol in Cushing's disease. A multicenter study revealed that whereas LCI699 did normalize CYP11B1-produced cortisol levels as desired, a simultaneous decrease in aldosterone was observed, likely partially due to simultaneous inhibition of CYP11B2 (30). However, a longer phase II trial did not note blood pressure changes, underscoring the complexities with poorly selective agents. Defining CYP11B1 preference for the *S* conformation paves the way for more selective drug design for the treatment of Cushing's disease.

The substrates of CYP11B1 and CYP11B2 are 11-deoxycortisol and 11-deoxycorticosterone, respectively. Whereas CYP11B1 is an efficient 11β-hydroxylase (Fig. S3), CYP11B2 performs 11β-hydroxylation but is much better at subsequent C18 hydroxylation and 18-oxidation to generate aldosterone, although the latter reaction is poor (Fig. S4). The structure of CYP11B2 with 11-deoxycorticosterone reveals the steroidal core oriented lengthwise over the heme, with C18 4.02 Å and C11 4.23 Å from the iron. Comparison with the CYP11B1 structure reveals that, if unaltered, the side chain of Phe-130 would sterically hinder binding of 11-deoxycorticosterone or 11-deoxycortisol with the orientation shown in CYP11B2, pushing the steroidal core away from it. As a result, C11 would likely be the site of oxidation closest to the heme iron, consistent with its function. It has been suggested that CYP11B2 is poor at overall aldosterone production because the multiple intermediates may dissociate from CYP11B2 via an open channel observed from the active site to the protein surface (21). However, CYP11B1 also has a similar channel (Fig. 4) yet is very efficient at 11β-hydroxylation. This does not rule out differences in the conformational flexibility of the two proteins, but this idea should be investigated further, specifically with substrates and redox partner proteins that could modulate conformational changes. Regardless, the current structure also provides a context for evaluating naturally occurring CYP11B1 mutations that occur throughout the enzyme and cause disease in patients (19).

Conclusions

Overall, the CYP11B1 structure revealed crucial structural distinctions from CYP11B2 that underlie inhibitor binding and enzyme function and help rationalize the impact of disease-associated mutations while yielding valuable guidance in more

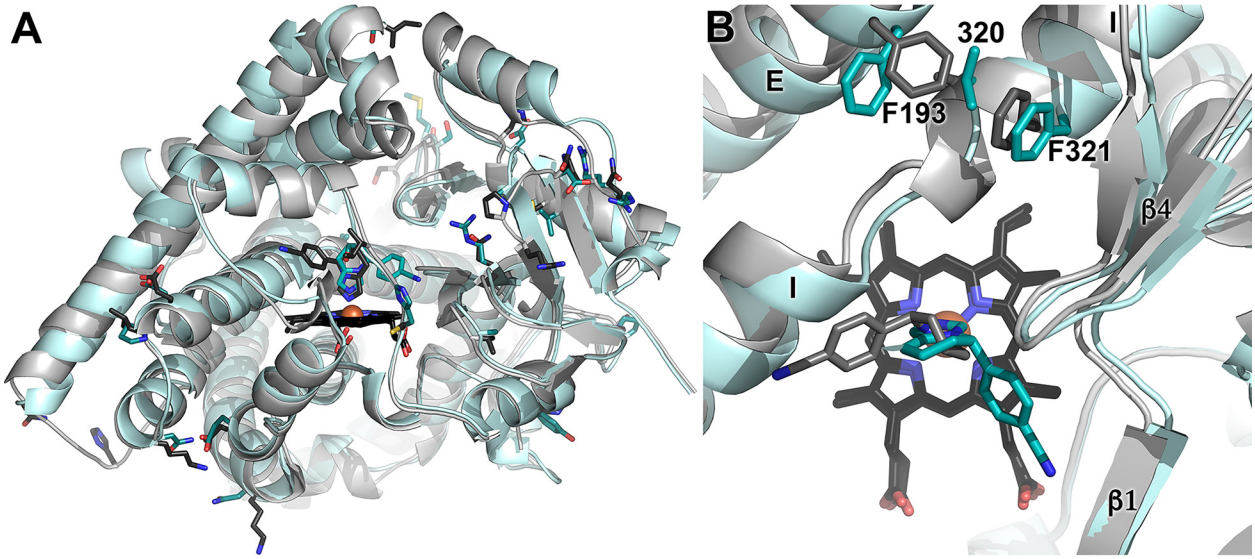

Figure 3. CYP11B1 (*light cyan*) and CYP11B2 (*gray*) structure comparison. *A*, nonidentical amino acids (*darker sticks* with *red* for oxygen atoms and *blue* for nitrogen atoms) are relatively distant from the active site and/or face outward, like residue 112 just *above* fadrozole. *B*, differences in the I helix conformation occur adjacent to residue 320, which is Val in CYP11B1 and Ala in CYP11B2 (PDB code 4FDH).

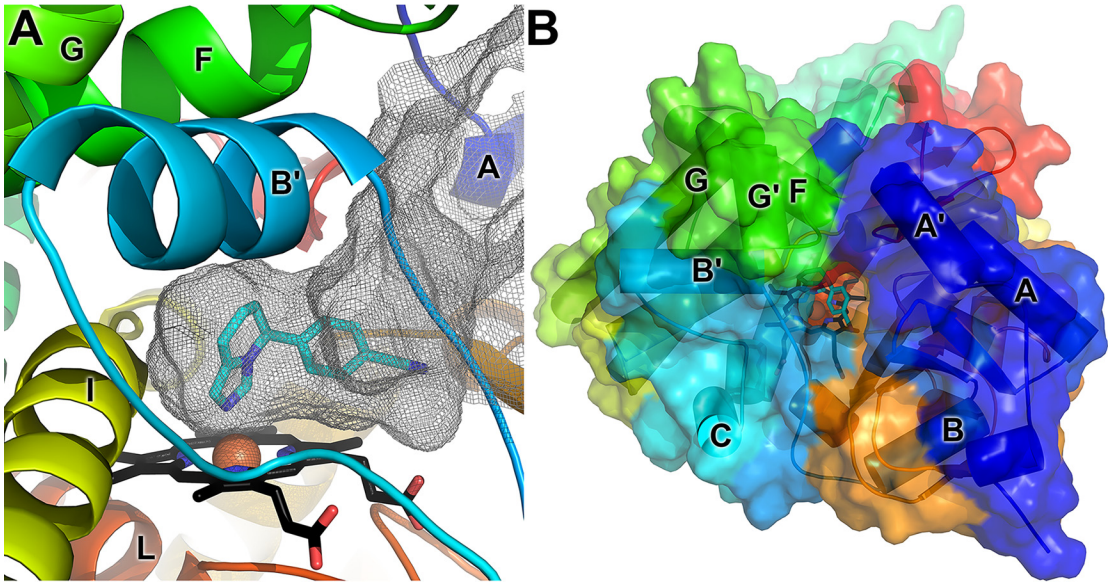

Figure 4. CYP11B1 channel. *A*, the active site is connected to a channel (*gray mesh*) all the way to the protein surface. *B*, the opening of this channel is flanked by the A′ helix, the B/B′ loop, and the F/G′ region.

selective drug design for Cushing's disease, hypertension, and breast cancer.

Experimental procedures

Materials

Racemic fadrozole hydrochloride (CAS 102676-31-3) and 11-deoxycortisol (CAS 152-58-9) were purchased from Sigma-Aldrich.

Protein expression and purification

CYP11B1—A synthetic, codon-optimized cDNA for CYP11B1 expression was generated (Blue Heron Biotech, Bothell, WA). This construct coded for a truncated protein with MATK prior to the 27th amino acid of the WT sequence and a His_4 tag at the C terminus. This gene was cloned into the pCWori vector, and the resulting construct was transformed into the *E. coli* strain DH5α already containing the pGro7 vector encoding the GroEL/ES chaperone. The construct was later modified to code for the sequence MAKKTSS prior to the 31st amino acid of the WT sequence (Fig. S5). A single colony from a lysogeny broth (LB) agar plate containing 100 μg/ml carbenicillin for pCW selection and 20 μg/ml chloramphenicol for pGro7 selection was used to initiate a 30-ml LB starter grown at 37 °C with the same antibiotics. For expression, 800 ml of terrific broth (TB) with 2× potassium phosphate buffer and respective antibiotics in a 2.8-liter Fernbach flask were inoculated with 8 ml of overnight culture and incubated at 37 °C and 220 rpm until A_{600} of 0.4–0.6 was reached. CYP11B1 expression was then induced with 1 mM isopropyl β-D-1-thiogalactopyranoside (IPTG) and expression of the GroEL/ES chaperone with 4 mg/ml arabinose.

At this point, cultures were supplemented with 1 mM δ-aminolevulinic acid heme precursor. Protein expression was carried out at 27 °C at 190 rpm for 48 h, after which bacterial pellets were collected by centrifugation at 6,000 rpm and 4 °C for 15 min. The cell pellet was resuspended in lysis buffer (50 mM potassium phosphate buffer (pH 7.4), 20% (v/v) glycerol, 500 mM sodium acetate, 1.5% (w/v) sodium cholate, 1.5% (v/v) Tween 20, 0.1 mM PMSF, 0.1 mM DTT), and the cells were disrupted by passage through a French press with one pass at 16,000 p.s.i. The cell debris was removed by ultracentrifugation at 35,000 rpm for 50 min at 4 °C. The resulting supernatant was loaded on a Ni-NTA column (Ni/NTA Superflow, Qiagen) equilibrated with 3 CV of equilibration buffer (50 mM potassium phosphate buffer (pH 7.4), 20% (v/v) glycerol, 500 mM sodium acetate, 1% (w/v) sodium cholate, 1% (v/v) Tween 20, 0.1 mM PMSF, 0.1 mM DTT). The column was first washed with 5 CV of washing buffer I (50 mM potassium phosphate buffer (pH 7.4), 20% (v/v) glycerol, 500 mM sodium acetate, 1% (w/v) sodium cholate, 1% (v/v) Tween 20, 12 mM histidine, 0.1 mM PMSF, 0.1 mM DTT) and then with 5 CV of washing buffer II (50 mM potassium phosphate buffer (pH 7.4), 20% (v/v) glycerol, 1% (w/v) sodium cholate, 1% (v/v) Tween 20, 12 mM histidine, 0.1 mM PMSF, 0.1 mM DTT) containing 0.1 mM ATP to promote removal of GroEL/ES from the CYP11B1 protein. CYP11B1 protein was eluted with 80 mM histidine buffer (20 mM potassium phosphate buffer (pH 7.4), 20% (v/v) glycerol, 1% (w/v) sodium cholate, 1% (v/v) Tween 20, 80 mM histidine, 0.1 mM PMSF, 0.1 mM DTT) and concentrated in a 50-kDa centrifugal device. Subsequent cation-exchange chromatography employed a HiTrap SP FF column (GE Healthcare) equilibrated with 5 CV of buffer containing 20 mM potassium phosphate buffer (pH 7.4), 20% (v/v) glycerol, 1% (w/v) sodium cholate, 0.1% (v/v) Tween 20, 0.1 mM PMSF, and 0.1 mM DTT. After loading, the column was washed with 15 CV of equilibration buffer, and the protein was eluted with a gradient from 0 to 300 mM NaCl (50 mM potassium phosphate buffer (pH 7.4), 20% (v/v) glycerol, 1% (w/v) sodium cholate, 0.1% (v/v) Tween 20, 0.1 mM PMSF, 0.1 mM DTT, 0–300 mM NaCl). When the desired end product was inhibitor-saturated enzyme, all cation exchange and subsequent buffers were supplemented with 30 μM fadrozole dissolved in ethanol. The oligomeric state of CYP11B1 was examined by size-exclusion chromatography (GE Healthcare HiLoad® 16/60 Superdex® 200 pg) under detergent-depleting buffer conditions using 50 mM potassium phosphate buffer (pH 7.4), 20% (v/v) glycerol, and 500 mM NaCl. The resulting purified protein was flash-frozen and stored at −80 °C until further use. Purity was examined using SDS-PAGE analysis, and the ratio of absorbance of the Soret peak *versus* the total protein absorbance was determined at 280 nm. The R_Z for pure CYP11B1 saturated with fadrozole is usually ~1.1.

Adrenodoxin reductase—The pET17b plasmid with human adrenodoxin reductase cDNA containing a C-terminal 6-residue His tag was kindly provided by Dr. Richard Auchus. The expression vector was co-transformed with the pGro7 vector in C41(DE3), and transformed cells were grown on an LB agar plate containing 100 μg/ml carbenicillin for pET17b selection and 20 μg/ml chloramphenicol for pGro7 selection. A single colony from the agar plate was used to grow a 30-ml starter culture with respective antibiotics in LB medium at 37 °C for 5 h. For expression cultures, 1 liter of TB medium in 2.8-liter Fernbach flasks was inoculated with 25 ml of starter culture and grown at 37 °C and 250 rpm. At an A_{600} of 0.5, expression of adrenodoxin reductase was induced with 100 mg/liter IPTG and the chaperones with 3 g/liter arabinose. The cells were also supplemented with 0.1 mg/liter riboflavin 5-phosphate to support FAD synthesis. Cultures were incubated for 40 h at 20 °C and 140 rpm. After collecting the cells at 6,000 rpm at 4 °C for 15 min, the cell pellet was resuspended in lysis buffer (50 mM potassium phosphate buffer, pH 7.4, 300 mM NaCl, 20% (v/v) glycerol, 10 μM FAD, 0.1 mM PMSF) and disrupted by a French press with one pass at 16,000 p.s.i. The cell debris was removed by ultracentrifugation at 35,000 rpm for 50 min at 4 °C, and the supernatant was loaded on a Ni-NTA column, which was previously equilibrated with 3 CV of lysis buffer. The column was washed with 6 CV of lysis buffer, and reductase eluted with a histidine gradient from 0 to 80 mM, during which the main reductase fraction eluted at ~40 mM histidine. The eluted protein was concentrated in a 50-kDa centrifugal device for subsequent size-exclusion chromatography using 50 mM potassium phosphate, pH 7.4, 300 mM NaCl, and 20% (v/v) glycerol as a buffer. Eluting adrenodoxin reductase was identified by an absorbance at 450 and 280 nm. The respective fractions were pooled and concentrated, and the buffer was exchanged to storage buffer consisting of 50 mM potassium phosphate buffer (pH 7.4) and 20% (v/v) glycerol. The protein was flash-frozen and stored at −80 °C. Purity was analyzed by SDS-PAGE analysis as well as spectral analysis of the ratio of the total protein absorbance at 270 nm *versus* the FAD absorbance maximum at 450 nm. At a value of 7.8, the protein is considered to be pure (31). Adrenodoxin reductase concentration was determined using the extinction coefficient at the absorbance maximum at 450 nm ($\epsilon = 11.3\ mM^{-1}\ cm^{-1}$) according to the Beer–Lambert law. Using this method, adrenodoxin reductase could be obtained with a final yield of 160 nmol/liter expression culture.

Adrenodoxin—A pLW plasmid containing coding for human adrenodoxin with a six-residue N-terminal histidine tag was kindly provided by Dr. Richard Auchus. The expression vector was transformed into C41(DE3) cells, and cells were plated on LB agar containing 100 μg/ml carbenicillin for plasmid selection. A starter culture was grown from a single colony in 30 ml of LB medium supplemented with 100 μg/ml carbenicillin at 37 °C overnight.

For expression, 1 liter of TB medium in a 2.8-liter Fernbach flask was inoculated with 10 ml of starter culture and grown at 37 °C and 250 rpm. At A_{600} of 0.4–0.6, adrenodoxin expression was induced with 1 mM IPTG, after which cultures were incubated at 28 °C for an additional 20 h.

After cell collection by centrifugation at 6,000 rpm at 4 °C for 15 min, the cells were resuspended in lysis buffer (50 mM potassium phosphate buffer, pH 7.4, 300 mM NaCl, 5% (v/v) glycerol, 0.1 mM PMSF) and disrupted by a French press with one pass at 16,000 p.s.i. After ultracentrifugation at 35,000 rpm for 50 min at 4 °C, the supernatant was loaded on a 30-ml Ni-NTA column (Qiagen) equilibrated with lysis buffer. The column was washed with 8 CV of 50 mM potassium phosphate buffer, pH 7.4, 300 mM NaCl, 5% (v/v) glycerol, 4 mM histidine, and 0.1 mM PMSF,

and the adrenodoxin was eluted with 5 CV of the same buffer containing 80 mM histidine. Fractions containing adrenodoxin were identified by a higher absorbance at 414 nm, pooled, concentrated in a 10-kDa centrifugal device, and then diluted 5-fold with binding buffer (50 mM potassium phosphate buffer, pH 7.4, 5% (v/v) glycerol, and 0.1 mM PMSF) to decrease the salt concentration. For anion-exchange chromatography, two connected 1-ml HiTrap Q columns (FF) were equilibrated with 10 CV binding buffer. The protein was loaded, washed with 5 CV of binding buffer and then with 20 CV of the same buffer containing 60 mM NaCl, and eluted with 15 CV of binding buffer increased to 300 mM NaCl. Fractions exhibiting an absorbance at 414 nm and 280 nm were concentrated, and the buffer was exchanged to 50 mM potassium phosphate buffer, pH 7.4, with 5% (v/v) glycerol at −80 °C. Purity was verified by SDS-PAGE analysis as well as the analysis of the absorbance spectrum. The absorbance ratio of the iron–sulfur cluster at 414 nm *versus* the total protein absorbance at 276 nm of 0.8 was considered to reflect a pure adrenodoxin sample. Adrenodoxin concentration was determined using the extinction coefficient at the absorbance maximum at 414 nm ($\epsilon = 11\ mM^{-1}\ cm^{-1}$) according to the Beer–Lambert law (32). Using this method, adrenodoxin could be obtained with a final yield of 2,000 nmol/liter expression culture.

Crystallization and structural determination

Initial crystals were grown from 0.5 μl of fadrozole-saturated (Soret maximum at 423.5 nm) purified CYP11B1 (50 mM potassium phosphate buffer (pH 7.4), 20% (v/v) glycerol, 500 mM NaCl; 30 mg/ml determined using the Soret absorbance maximum and $\epsilon = 100\ mM^{-1}\ cm^{-1}$) mixed with 0.5 μl of 0.1 M imidazole, pH 7.4, and 12% (v/v) PEG 20,000 in a sitting drop using the Crystal Gryphon Robot (Art Robbins Instruments, Sunnyvale, CA). These drops were equilibrated against 65 μl of the same imidazole solution at 20 °C. After 3 weeks, small crystal plates could be detected. A seed stock was prepared using 1 μl of these crystals mixed in 50 μl of the imidazole solution and stored at −80 °C until use. One μl of this seed stock was mixed with 1 μl of 40 mg/ml purified CYP11B1 for hanging-drop vapor-diffusion experiments against the same imidazole solution (500 μl) at 20 °C. Diffraction data were collected on beamline 12-2 of the Stanford Synchrotron Radiation Lightsource using Blu-Ice and processed using XDS (33) (Table 1). The CYP11B1 structure was solved by molecular replacement using Phaser (34) and a search model consisting of CYP11B2 in complex with fadrozole (PDB entry 4FDH (21)). Model building and refinement were performed iteratively with Coot (35) and Phenix (36), respectively (Table 1). The ligand fadrozole was generated using elBOW in Phenix (36). Figures were generated with PyMOL (37). Atomic coordinates and structure factors for the reported CYP11B1 crystal structures have been deposited with the Protein Data Bank under accession code 6M7X.

In vitro activity assays

To determine the catalytic function of CYP11B1, *in vitro* activity assays were performed with the physiological substrate 11-deoxycortisol. First a stock of 100 μM 1,2-dilauroyl-*sn*-glycero-3-phosphocholine was prepared in 50 mM HEPES buffer (pH 7.4) and sonicated for 5 min to promote micelle formation. The mitochondrial redox system was reconstituted in a total reaction volume of 500 μl using 1 μM CYP11B1, 1 μM adrenodoxin reductase, and 40 μM adrenodoxin. The conversion of 200 μM 11-deoxycortisol (dissolved in ethanol) was started with 5 mM NADPH. The reaction was quenched with chloroform. Steroids were extracted twice with chloroform, dried, resuspended in 20% (v/v) acetonitrile, and analyzed on a reversed-phase HPLC column (Phenomenex, Luna®, 5 μm, C18, 150 × 4.6 mm) using an acetonitrile–water gradient as follows (phase A: 10% (v/v) acetonitrile; phase B: 100% acetonitrile): 0–5 min, 20% B (step); 6–15 min, 40% B (step); 16–18 min, 80% B (step); 19–25 min, 20% B (step) at 40 °C and a flow rate of 0.8 ml/min. Steroids were analyzed by a UV-visible detector at an absorbance of 240 nm. Standards for cortisol and 11-deoxycortisol were used to determine the retention time, which was 10.3 min for 11-deoxycortisol and 8.3 min for cortisol.

Table 1
X-ray data collection, refinement, and validation statistics for CYP11B1/fadrozole
Values for the highest-resolution shell are shown in parenthesis.

Data collection	
Space group	I4
Cell dimensions	
a, *b*, *c* (Å)	140.57, 140.57, 145.78
α, β, γ (degrees)	90.0, 90.0, 90.0
Resolution (Å)	38.45–2.10 (2.21–2.10)
Redundancy	6.7 (5.2)
R_{pim}	0.038 (0.443)
Mn(*I*/sd)	10 (1.5)
Completeness (%)	99.5 (96.6)
Total/unique reflections	553,646/82,404 (60,667/11,667)
Refinement	
Resolution (Å)	38.45–2.10
No. of reflections	82,037
R_{work}/R_{free}	18.9/21.8
Molecules per asymmetric unit	2
Residues modeled for each molecule	
A	34–281, 287–502
B	34–280, 286–502
No. of non-hydrogen atoms/*B* factor	
Protein	7,496/51.7
Ligand	34/53.6
Heme	86/34.3
Water	428/52.4
Root mean square deviations	
Bond lengths (Å)	0.003
Bond angles (degrees)	0.54
Coordinate error (maximum likelihood) (Å)	0.30
Structure analysis	
Ramachandran plot: preferred/allowed/outliers (%)	96.9/2.85/0.55/0.0
Root mean square deviation between molecules in the asymmetric unit	0.325

Author contributions—E. E. S. and S. B.-A. conceived the study, performed data analysis, and wrote the manuscript. S. B.-A. conducted experiments.

Acknowledgments—X-ray data were collected at the Stanford Synchrotron Radiation Lightsource (SSRL). The SSRL Structural Molecular Biology Program is supported by the United States Department of Energy Office of Biological and Environmental Research and by the National Institutes of Health, NCRR, Biomedical Technology Program, and NIGMS. Linda Blake assisted with the design of the original CYP11B1 expression construct and established an initial expression and purification protocol. Constructs for expression of adrenodoxin and adrenodoxin reductase were gifts from Dr. Richard Auchus (University of Michigan).

References

1. Denver, R. J. (2009) Structural and functional evolution of vertebrate neuroendocrine stress systems. *Ann. N.Y. Acad. Sci.* **1163,** 1–16 CrossRef Medline
2. Panagiotakopoulos, L., and Neigh, G. N. (2014) Development of the HPA axis: where and when do sex differences manifest? *Front. Neuroendocrinol.* **35,** 285–302 CrossRef Medline
3. Bellavance, M. A., and Rivest, S. (2014) The HPA-immune axis and the immunomodulatory actions of glucocorticoids in the brain. *Front. Immunol.* **5,** 136 Medline
4. Kirk, L. F., Jr., Hash, R. B., Katner, H. P., and Jones, T. (2000) Cushing's disease: clinical manifestations and diagnostic evaluation. *Am. Fam. Physician* **62,** 1119–1127, 1133–1134 Medline
5. Pivonello, R., De Martino, M. C., De Leo, M., Lombardi, G., and Colao, A. (2008) Cushing's syndrome. *Endocrinol. Metab. Clin. North Am.* **37,** 135–149, ix CrossRef Medline
6. Unuane, D., Tournaye, H., Velkeniers, B., and Poppe, K. (2011) Endocrine disorders & female infertility. *Best Pract. Res. Clin. Endocrinol. Metab.* **25,** 861–873 CrossRef Medline
7. Te Riet, L., van Esch, J. H., Roks, A. J., van den Meiracker, A. H., and Danser, A. H. (2015) Hypertension: renin-angiotensin-aldosterone system alterations. *Circ. Res.* **116,** 960–975 CrossRef Medline
8. Piaditis, G., Markou, A., Papanastasiou, L., Androulakis, I. I., and Kaltsas, G. (2015) Progress in aldosteronism: a review of the prevalence of primary aldosteronism in pre-hypertension and hypertension. *Eur. J. Endocrinol.* **172,** R191–R203 CrossRef Medline
9. Lackland, D. T., and Weber, M. A. (2015) Global burden of cardiovascular disease and stroke: hypertension at the core. *Can. J. Cardiol.* **31,** 569–571 CrossRef Medline
10. Ballinger, T. J., Meier, J. B., and Jansen, V. M. (2018) Current landscape of targeted therapies for hormone-receptor positive, HER2 negative metastatic breast cancer. *Front. Oncol.* **8,** 308 CrossRef Medline
11. Hille, U. E., Zimmer, C., Haupenthal, J., and Hartmann, R. W. (2011) Optimization of the first selective steroid-11β-hydroxylase (CYP11B1) inhibitors for the treatment of cortisol dependent diseases. *ACS Med. Chem. Lett.* **2,** 559–564 CrossRef Medline
12. Hille, U. E., Zimmer, C., Vock, C. A., and Hartmann, R. W. (2011) First selective CYP11B1 inhibitors for the treatment of cortisol-dependent diseases. *ACS Med. Chem. Lett.* **2,** 2–6 CrossRef Medline
13. Zhu, W., Chen, Z., Li, Q., Tan, G., and Hu, G. (2016) Inhibitors of 11β-hydroxylase (CYP11B1) for treating diseases related to excess cortisol. *Curr. Med. Chem.* **23,** 623–633 CrossRef Medline
14. Emmerich, J., van Koppen, C. J., Burkhart, J. L., Engeli, R. T., Hu, Q., Odermatt, A., and Hartmann, R. W. (2018) Accelerated skin wound healing by selective 11β-hydroxylase (CYP11B1) inhibitors. *Eur. J. Med. Chem.* **143,** 591–597 CrossRef Medline
15. Emmerich, J., van Koppen, C. J., Burkhart, J. L., Hu, Q., Siebenbürger, L., Boerger, C., Scheuer, C., Laschke, M. W., Menger, M. D., and Hartmann, R. W. (2017) Lead optimization generates CYP11B1 inhibitors of pyridylmethyl isoxazole type with improved pharmacological profile for the treatment of Cushing's disease. *J. Med. Chem.* **60,** 5086–5098 CrossRef Medline
16. Emmerich, J., Hu, Q., Hanke, N., and Hartmann, R. W. (2013) Cushing's syndrome: development of highly potent and selective CYP11B1 inhibitors of the (pyridylmethyl)pyridine type. *J. Med. Chem.* **56,** 6022–6032 CrossRef Medline
17. Bernhardt, R. (2016) The potential of targeting CYP11B. *Expert Opin. Ther. Targets* **20,** 923–934 CrossRef Medline
18. Yu, R., Wang, J., Wang, R., Lin, Y., Hu, Y., Wang, Y., Shu, M., and Lin, Z. (2015) Combined pharmacophore modeling, 3D-QSAR, homology modeling and docking studies on CYP11B1 inhibitors. *Molecules* **20,** 1014–1030 CrossRef Medline
19. Khattab, A., Haider, S., Kumar, A., Dhawan, S., Alam, D., Romero, R., Burns, J., Li, D., Estatico, J., Rahi, S., Fatima, S., Alzahrani, A., Hafez, M., Musa, N., Razzghy Azar, M., *et al.* (2017) Clinical, genetic, and structural basis of congenital adrenal hyperplasia due to 11beta-hydroxylase deficiency. *Proc. Natl. Acad. Sci. U.S.A.* **114,** E1933–E1940 CrossRef Medline
20. Abbaszadegan, M. R., Hassani, S., Vakili, R., Saberi, M. R., Baradaran-Heravi, A., A'Rabi, A., Hashemipour, M., Razzaghi-Azar, M., Moaven, O., Baratian, A., Ahadian, M., Keify, F., and Meurice, N. (2013) Two novel mutations in CYP11B1 and modeling the consequent alterations of the translated protein in classic congenital adrenal hyperplasia patients. *Endocrine* **44,** 212–219 CrossRef Medline
21. Strushkevich, N., Gilep, A. A., Shen, L., Arrowsmith, C. H., Edwards, A. M., Usanov, S. A., and Park, H. W. (2013) Structural insights into aldosterone synthase substrate specificity and targeted inhibition. *Mol. Endocrinol.* **27,** 315–324 CrossRef Medline
22. Browne, L. J., Gude, C., Rodriguez, H., Steele, R. E., and Bhatnager, A. (1991) Fadrozole hydrochloride: a potent, selective, nonsteroidal inhibitor of aromatase for the treatment of estrogen-dependent disease. *J. Med. Chem.* **34,** 725–736 CrossRef Medline
23. Martin, R. E., Aebi, J. D., Hornsperger, B., Krebs, H. J., Kuhn, B., Kuglstatter, A., Alker, A. M., Märki, H. P., Müller, S., Burger, D., Ottaviani, G., Riboulet, W., Verry, P., Tan, X., Amrein, K., and Mayweg, A. V. (2015) Discovery of 4-aryl-5,6,7,8-tetrahydroisoquinolines as potent, selective, and orally active aldosterone synthase (CYP11B2) inhibitors: *in vivo* evaluation in rodents and cynomolgus monkeys. *J. Med. Chem.* **58,** 8054–8065 CrossRef Medline
24. Roumen, L., Sanders, M. P., Pieterse, K., Hilbers, P. A., Plate, R., Custers, E., de Gooyer, M., Smits, J. F., Beugels, I., Emmen, J., Ottenheijm, H. C., Leysen, D., and Hermans, J. J. (2007) Construction of 3D models of the CYP11B family as a tool to predict ligand binding characteristics. *J. Comput. Aided Mol. Des.* **21,** 455–471 CrossRef Medline
25. Curnow, K. M., Mulatero, P., Emeric-Blanchouin, N., Aupetit-Faisant, B., Corvol, P., and Pascoe, L. (1997) The amino acid substitutions Ser288Gly and Val320Ala convert the cortisol producing enzyme, CYP11B1, into an aldosterone producing enzyme. *Nat. Struct. Biol.* **4,** 32–35 CrossRef Medline
26. Bechtel, S., Belkina, N., and Bernhardt, R. (2002) The effect of amino-acid substitutions I112P, D147E and K152N in CYP11B2 on the catalytic activities of the enzyme. *Eur. J. Biochem.* **269,** 1118–1127 CrossRef Medline
27. Böttner, B., Denner, K., and Bernhardt, R. (1998) Conferring aldosterone synthesis to human CYP11B1 by replacing key amino acid residues with CYP11B2-specific ones. *Eur. J. Biochem.* **252,** 458–466 CrossRef Medline
28. Rigel, D. F., Fu, F., Beil, M., Hu, C. W., Liang, G., and Jeng, A. Y. (2010) Pharmacodynamic and pharmacokinetic characterization of the aldosterone synthase inhibitor FAD286 in two rodent models of hyperaldosteronism: comparison with the 11β-hydroxylase inhibitor metyrapone. *J. Pharmacol. Exp. Ther.* **334,** 232–243 CrossRef Medline
29. Furet, P., Batzl, C., Bhatnagar, A., Francotte, E., Rihs, G., and Lang, M. (1993) Aromatase inhibitors: synthesis, biological activity, and binding mode of azole-type compounds. *J. Med. Chem.* **36,** 1393–1400 CrossRef Medline
30. Bertagna, X., Pivonello, R., Fleseriu, M., Zhang, Y., Robinson, P., Taylor, A., Watson, C. E., Maldonado, M., Hamrahian, A. H., Boscaro, M., and Biller, B. M. (2014) LCI699, a potent 11β-hydroxylase inhibitor, normalizes urinary cortisol in patients with Cushing's disease: results from a multicenter, proof-of-concept study. *J. Clin. Endocrinol. Metab.* **99,** 1375–1383 CrossRef Medline
31. Sagara, Y., Wada, A., Takata, Y., Waterman, M. R., Sekimizu, K., and Horiuchi, T. (1993) Direct expression of adrenodoxin reductase in *Escherichia coli* and the functional characterization. *Biol. Pharm. Bull.* **16,** 627–630 CrossRef Medline
32. Coghlan, V. M., and Vickery, L. E. (1989) Expression of human ferredoxin and assembly of the [2Fe-2S] center in *Escherichia coli*. *Proc. Natl. Acad. Sci. U.S.A.* **86,** 835–839 CrossRef Medline

33. Kabsch, W. (2010) XDS. *Acta Crystallogr. D Biol. Crystallogr.* **66,** 125–132 CrossRef Medline
34. McCoy, A. J., Grosse-Kunstleve, R. W., Adams, P. D., Winn, M. D., Storoni, L. C., and Read, R. J. (2007) Phaser crystallographic software. *J. Appl. Crystallogr.* **40,** 658–674 CrossRef Medline
35. Emsley, P., Lohkamp, B., Scott, W. G., and Cowtan, K. (2010) Features and development of Coot. *Acta Crystallogr. D Biol. Crystallogr.* **66,** 486–501 CrossRef Medline
36. Adams, P. D., Afonine, P. V., Bunkóczi, G., Chen, V. B., Davis, I. W., Echols, N., Headd, J. J., Hung, L. W., Kapral, G. J., Grosse-Kunstleve, R. W., McCoy, A. J., Moriarty, N. W., Oeffner, R., Read, R. J., Richardson, D. C., *et al.* (2010) PHENIX: a comprehensive Python-based system for macromolecular structure solution. *Acta Crystallogr. D Biol. Crystallogr.* **66,** 213–221 CrossRef Medline
37. DeLano, W. L. (2017) *The PyMOL Molecular Graphics System*, version 1.8.6.2, Schroedinger, LLC, New York